Nigerian Journal of Physics (NJP)
ISSN online: 3027-0936
ISSN print: 1595-0611
DOI: https://doi.org/10.62292/njp.v33i1.2024.183
Volume 33(1), March 2024

Examining the Variations in the Properties of Chemically Pulverized Carbons from Cocos Nucifera across Nigeria's Six Political Zones

***[1]Ajibade, I. I. [2]Babaji, G., [2]Gidado, A. S., [3]Paiman, S. [3]Sin Tee, T., [3]Md. Shazlly and [4]Adekunle, A. S.**

[1]Department of Physics, Federal University Gusau, Nigeria.
[2]Department of Physics, Bayero University Kano, Nigeria.
[3]Department of physics, Faculty of Science, Universiti Putra Malaysia
[4]Department of Chemistry, Obafemi Awolowo University Ile-Ife

*Corresponding author's email: Isaajibade@fugusau.edu.ng
ORCID: https://orcid.org/0000-0003-1586-666X

ABSTRACT

High-power, renewable energy sources are needed to power the growing number of portable electronics and hybrid cars. Reassessing the pyrolysis of biomass, especially from easily accessible African tall coconut shells (Cocos nucifera), is a viable way to both meet energy needs and slow down global warming. This work describes a novel method for producing activated carbon from coconut shells obtained from six different regions of Nigeria by combining chemical pulverization and pyrolysis. After lignin was eliminated from the ground-up samples using sulfuric acid, they were pyrolyzed at different temperatures (650–850°C). To clarify the physicochemical characteristics of the activated carbons, a variety of sophisticated characterization methods were used, such as Fourier Transform Infrared (FTIR), X-ray diffraction (XRD), Raman spectroscopy, Field Emission Scanning Electron Microscopy (FESEM), and Brunauer-Emmett-Teller (BET) analysis. The findings showed an intriguing interaction between relative humidity and pyrolysis temperature which implies that moisture content of the precursor material plays a significant role in its viability for supercapacitor applications.

Keywords:
Biomass,
Chemical pulverization,
Lignin,
Cocos nucifera,
Pyrolysis,
Relative humidity.

INTRODUCTION

Supercapacitors, or electrochemical capacitors, have attracted a lot of attention from the scientific and technological community because of their intriguing potential as energy storage devices. However, compared to other storage options such as batteries, supercapacitors have a lower energy density of less than 10 Wh/kg (Hall et al., 2010). This limitation limits their widespread application in renewable energy installations, industrial energy control, backup power supplies, and hybrid electric cars. Several efforts have been made to develop nanostructured active electrode materials in order to increase the energy density of supercapacitors (Zhang et al., 2010). These materials are designed to have sufficient porosity, surface area, and shape, which increases energy density without compromising their high-power density and durability. Electrochemical systems (EC) can be used in accordance with the charge storage methods of the active materials utilized.

Since pseudo capacitors have substantially higher capacitance than EDLCs, they are frequently used in conjunction with EDLCs to increase energy density and power (Nankya et al., 2020). An electrical double-layer capacitor's electrode functions as its basic support structure and is a key factor in influencing the stability and overall performance of supercapacitors. Supercapacitors use a broad range of electrode materials, each of which exhibits unique capacitance properties and performance features. Materials with large specific surface areas and pore volumes, such mesoporous and microporous materials, are especially desirable for electrode fabrication. Many research groups have attempted to produce electrodes from different carbon sources (Gao et al., 2020).

In the supercapacitor electrode market, activated carbon (AC) continues to be the material of choice despite a great deal of research and development. Its remarkable qualities—such as a high specific surface area (SSA), affordability, and consistent electrochemical performance and stability—are the reason for this

selection (Zhai et al., 2011). Supercapacitors (SC) can benefit from a variety of carbon-based electrode materials because of their large surface area, porosity, and surface functional groups. As an example, consider carbon composites, carbon generated from carbides, and aerogels containing carbons (Lee et al., 2014). Activated carbon (AC)-based materials are generally thought to have higher packing density, stronger chemical and physical stability, more porosity, and an enhanced surface area (Lekakou et al., 2011). The material's surface area and stability are the main causes of the high capacitance values (Dhillon &vonWuehlisch,2013).

When it comes to energy applications, biomass is a viable and sustainable source of materials that can replace fossil fuels. At the moment, it accounts for roughly 14% of overall energy consumption and roughly 35% of cooking and heating energy consumption, especially in third-world nations, especially in Africa (Onwumelu, 2023). Because biomass resources are readily available, abundant, naturally renewable, and environmentally benign, using them as electrodes in supercapacitor applications has gained popularity (Elmouwahidi et al., 2017).Many biomasses have been studied for their potential to produce porous activated carbon that can be used in industrial settings, such as sugarcane bagasse, rice husks, corn cobs and maize (Chen et al., 2017). Activated carbons, which have different surface areas, are used in industrial settings for a variety of purposes such as energy storage, removing toxic materials, purifying and separating materials in liquid and gaseous media, and acting as catalysts or supports for catalysts (Yakout & El-Deen, 2016). lowering carbon dioxide levels, eliminating odors, and eliminating dyes (Zhang et al., 2022). Alternative ecological biomass materials have been investigated as possible carbon reservoirs for use in supercapacitors. Examples of these materials include eggshells, wood sawdust, pistachio shells (as an example, see the cigarette filter), sunflower seed husk, and rice husk (Kumagai et al., 2013). When there are constraints on the ordered migration of crystalline elements in porous activated carbons made from coconut shells, graphene layers are oriented randomly, which eventually produces an amorphous structure (Ozoemena & Chen, 2016).

The internal surface area of pores created by micropores and mesopores is the main source of surface area in activated carbons (Das, & Meikap, 2015). Hierarchical porous structure, similar to other uses, is desirable in the context of non-faradaic electrical storage applications. The geometry, crystal structure, porosity, and surface characteristics of these carbon structures can all be tailored to satisfy particular needs. Many strategies, including as chemical activation, mild oxidation, template approaches, and mechanical, chemical, and thermal processes, can be used to accomplish this customization (Roberts et al., 2010). Physical or chemical approaches can be used to activate carbon compounds (Yang et al., 2023). To improve the stability and efficiency of EDL supercapacitors, it is advantageous to get very pure activated porous carbon materials free of contaminants (Sammed et al., 2023). Reductive deposition of heavy or alkali metals, which can cause short circuits, is less likely to occur when impurity levels are lowered (Fang et al., 2023). Additionally, by avoiding self-discharge, it helps to preserve a longer shelf life.

However, in the context of creating supercapacitors, it is necessary to take into account extraneous elements such the age, breed, and relative humidity of coconut shells and their possible impact on the usefulness of coconut shell as a precursor for activated carbon.

The measurement of the air's moisture content relative to its maximum capacity at a given temperature is called relative humidity, or RH. According to Abdullah et al. (2023), it is stated as a percentage that ranges from 0% (totally dry air) to 100% (air saturated with water vapor). RH is equal to (Saturation vapor pressure / Actual vapor pressure) × 100%. relative humidity (given in percentage terms) The current amount of water vapor in the air, expressed in measures such as millibars (mb) or hPa, is known as the actual vapor pressure.

It is true that biomass is influenced by relative humidity (RH), especially when considering ecosystems and plant growth. RH can have a big effect on biomass, and it depends on a lot of different things (Rippel et al., 2020). Plant transpiration rate is influenced by relative humidity (De Groeve et al., 2023). Plants release water vapor into the atmosphere through a process called transpiration. A plant may lose more water when the relative humidity is low, the air is dryer, and the gradient for the movement of water vapor from the plant to the atmosphere is steeper. This could result in the plant wilting, stunted growth, or even death (Zhang et al., 2023).

Low relative humidity is frequently linked to dry or drought situations (Mahmoud et al., 2023). Extended durations of low relative humidity can cause drought stress in plants, which can lower biomass production and possibly even cause plant death (Cotrina Cabello et al., 2023). Once more, higher relative humidity (RH) encourages less transpiration, or the loss of water from leaves. This conserves water and is advantageous for drought-tolerant plants or dry conditions. Within microclimates, there can be variations in relative humidity. These variations can impact the kinds of plants that flourish in each location, which can then have an impact on the distribution and productivity of biomass overall in the ecosystem (Van et al., 2023). In the current study, a chemical pulverization process with variable relative humidity is used to manufacture increased porous carbon from coconut shells from

diverse geopolitical zones in Nigeria. The coconut shells were treated with strong sulfuric acid before being activated. It has been discovered that treating materials with sulfuric acid effectively hydrolyzes and oxidizes them, adding a large number of functional groups to the carbon surface. Among these functional groups are Sulphur, phenolic, carboxyl, and lactone, among others. It has been shown that these functional groups improve the efficiency of electron and charge transfer activities that are connected to both faradaic and non-faradaic processes.

MATERIALS AND METHODS

Preparation of Activated Carbon

The following are the geographical locations of the six geopolitical zones in Nigeria where the coconut shell (CS) was obtained: SW (6.520N&3.380E), SS (4.820N&7.050E), SE (6.460N&7.610E), NW (12.940N&5.230E), NE (11.830N&13.150E), and NC (9.080N&7.400E). From these locations, the activated carbons (ACs) were prepared. After cleaning and sizing (to around 5 cm), the CS was dried for 24 hours at 80℃ in an oven. Using a 500μ sieve, the dry materials were crushed and separated. 1MH2SO4 was used as a chemical to functionalize the CS powder. After standing in a fume hood for 48 hours, the functionalized CS was cleaned with DI water until a pH of 6.5 was reached. After that, the sample was dried for eighteen hours at 120℃ in an electric oven. In a furnace with an argon environment, these six samples were activated at three (3) distinct temperatures, ramped at 10 0C/min, and held for two hours. The flow rate was 300 mL/min. At 650℃, the first part was engaged, and at 750℃ and 850℃, respectively, the second and third portions were heated.

Methodology for Characterization of Pulverized Carbon (AC)

The following characteristics were found in CS activated carbon samples that were collected at three distinct activation temperatures (650, 750, and 850 degrees Celsius) at six distinct geopolitical zones. FTIR analysis (PerkinElmer Spectrum) using the traditional KBr approach was used to determine the presence of different functional groups within the sample in the 600–4000 cm^{-1} range. X-Ray Diffraction (XRD) analysis was used to characterize the activated carbon products and examine their phase composition and crystallinity. Utilizing Co-Kα radiation (λ = 1.79 Å) and a BRUKER D8 ADVANCE X-RAY Diffractometer with a step size of 0.02° and a scan rate of 5°/min, the analysis was carried out in the 10–70° range. In order to determine if the activated carbon products contain ordered or disordered carbon, a PL micro-Raman spectrometer (model XMB3000-3000) with a 532 nm

Using an FEI NOVANANO SEM 450 device, field emission scanning electron microscopy (FESEM) examination was carried out to examine the surface morphology of activated carbon made from coconut shell. The samples prepared at various activation temperatures were examined in this analysis. The analysis examined the activated carbons' surface area and pore structure, building on earlier characterization techniques. This made use of nitrogen adsorption-desorption in liquid nitrogen at -196°C using a BET analyzer (Quanta chrome AUTOSORB-1). Samples were degassed at 200°C for six hours prior to analysis in order to guarantee precise measurements of total surface area, pore volume, pore diameter, and micropores and mesopores.

RESULTS AND DISCUSSION

The activated carbon's yield

The mass ratio of activated carbon generated to the mass of the raw material utilized is known as the yield. The study examined the impact of activation temperature on the yield of individual samples. It was observed that, as fig. 1 illustrates, the percentage yield falls as the activation time increases. The yield of product activated carbon is calculated by dividing the weight of the activated carbon product by the starting weight of the raw material used for activation. As the activation temperature rose from 650°C to 750°C and finally 850°C, the yield of activated carbons declined while the percentage of weight loss increased. A higher carbonization temperature causes more gasification reactions, which reduces yield (Foo & Hameed, 2012).

The carbon yield was calculated using.

$$\text{Percentage weight loss}=\frac{weight\ loss}{Original\ weight}\times 100 \quad (1)$$

$$\text{Percentage yield} = \frac{\boldsymbol{actual\ yield}}{\boldsymbol{theoretical\ yield}}\times 100 \quad (2)$$

Percentage weight loss

Table 1: Demonstrating how the temperature of activation affects the yield and weight loss and carbon yield of different activated carbon yields

SAMPLES	650 ℃	750 ℃	850 ℃	$R/H(\%)$
NE	11.5	33.3	69.3	38
SS	11	32.3	68.4	85
NC	11	31	71.5	65
NW	10	32.9	68	35
SW	11	32.9	70	85
SE	12	31.8	68.6	81
NE	88.5	66.7	30.7	38
SS	89	67.7	31.2	85
NC	89	69	28.5	65
NW	90	67.1	32	35
SW	89	67.1	30	85
SE	88	68.2	31.4	81

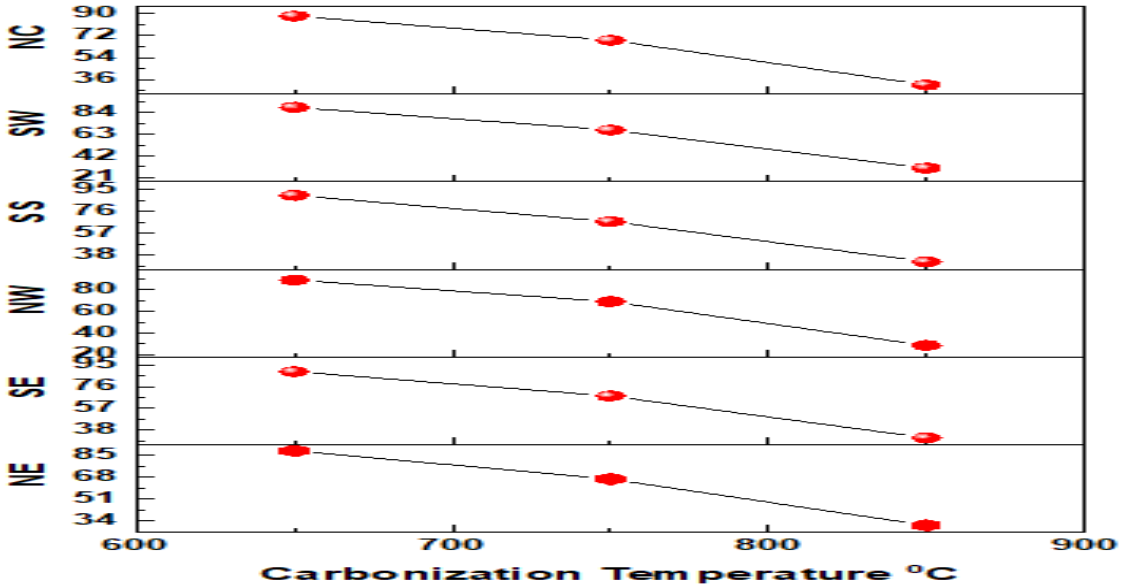

Figure 1. Impact of temperature during activation on different types of activated carbon yields

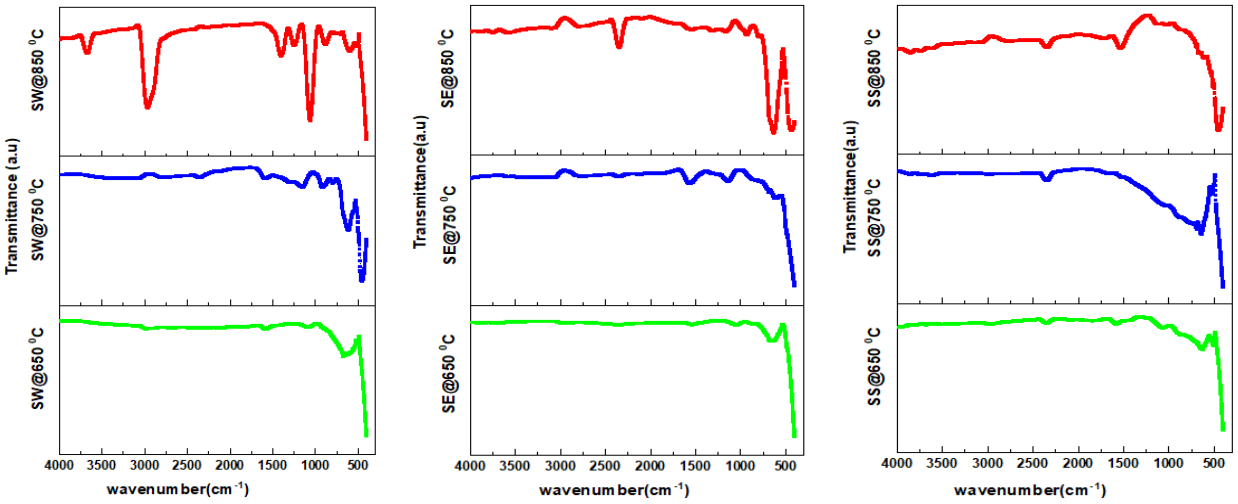

Figure 2: FTIR spectra of activated carbon generated at 650°C, 750°C, and 850°C, respectively, in SW, SE, and SS

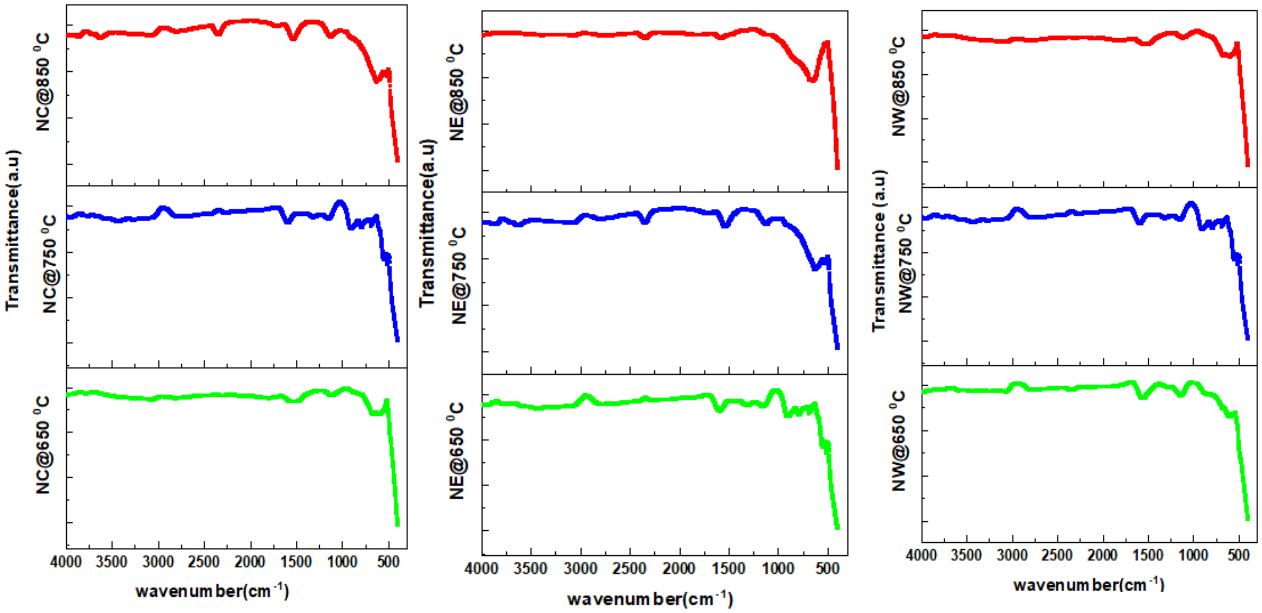

Figure 3: FTIR spectra of activated carbon made at 650°C, 750°C, and 850°C, respectively, in North Central, Northeast, and Northwest

The examination of surface functional group (FTIR)

The functional groups on the surface of activated carbon are responsible for its adsorption capabilities. The FTIR spectra of the activated carbon samples ACB@650, ACB@750, and ACB@850 are shown in Figure 2a. The amount of acidic functional groups decreases as the activation temperature rises, whereas the amount of basic surface groups on the carbon increases. For every assignment for both regions, the six samples all showed peaks at the same locations. The fingerprint region spanning from 1000 to 1500 cm-^{1} demonstrated the presence of aromatic compounds with strong and medium transmittance as well as C–C, C–OH, C–O, and C–N stretching concentrations. The stretching modes linked with the C–C and C–O bonds are represented by the peaks at 1080 and 1220 cm^{-1}, respectively. It is possible to credit the band at 2920.53 cm-1 to C–H bonds, most especially those present in methyl and methylene groups. The spectral band detected at 1625.48 cm-1 is ascribed to the vibrations of the C=C aromatic rings in polar functional groups. The band at 1415.95 cm-1 is attributed to the ion groups carboxylate and carbonyl.

This indicates that, similar to the effect of carbonization temperature, relative humidity during the synthesis of activated carbon affects the functional groups on the surface of the activated carbon products (Masthura & Abdul, 2018). The existence of a change in functional groups at 750°C in a region with lower relative humidity demonstrated the effect and influence of activation temperature on the chosen precursor (Sahu et al., 2023). When activated carbon is created in an inert atmosphere with a higher relative density, it displays a higher temperature-dependent array of functional groups in comparison to when it is formed at a lower relative density. This feature makes it more appropriate for a range of applications.

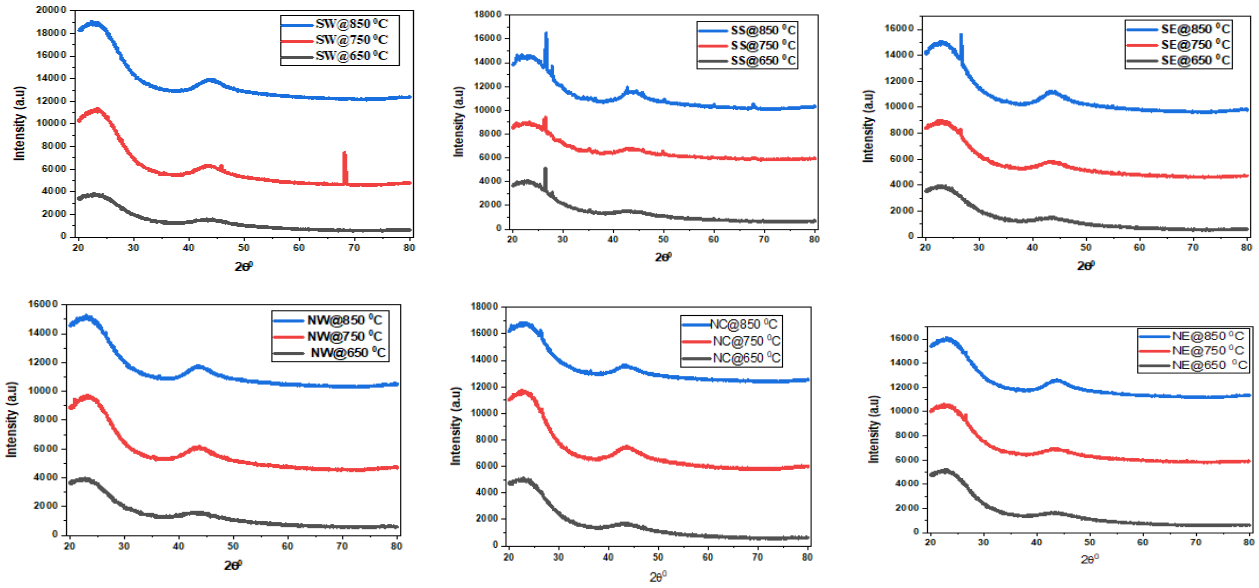

Figure 4. Activated carbon created in an inert atmosphere at three distinct temperatures: 650°C, 750°C, and 850°C. X-ray diffraction pattern

Analysis using X-ray diffraction (XRD).

Figure 4 shows the cocos nucifera samples' X-ray diffraction patterns. Because the coconut sample contained crystalline cellulose, two narrow, sharp peaks at 2θ values of approximately 16 and 22° for the biochar were seen (Jiang et al., 2007). As the pyrolysis temperature was raised, a wider peak appeared at 2θ values between 22 and 24°. At higher temperatures, however, the crystalline cellulose was destroyed. The coconut shell prepared at higher temperatures of 850°C showed the development of a large peak around 22 to 24°, which suggested the production of a crystalline structure with improved layer alignment. The temperature at which the pyrolysis occurred determined the physicochemical properties of the biochar that was produced. While the degree of carbonization increases in the ACB with RH less than 50% from 650°C to 750°C but depreciates at 850°C as increasing the pyrolysis temperature significantly increases the carbon content and decreases the oxygen and hydrogen contents of the biochar sample, the degree of carbonization of the ACB with RH greater than 60% was enhanced with successive increases in the pyrolysis temperature from 650 to 750 and 850°C (Chowdhury et al., 2016). A disordered graphitic sheet was the product of carbonization, which destroyed the graphitic structure at extremely high temperatures.

Table 2: Raman spectra of different pyrolysis temperatures for activated carbon (ACB-H2SO4)

SAMPLES	I_D	I_G	$\frac{I_D}{I_G}$
NC@650	1336	1600	0.83
NW@650	1337	1598	0.83
SE@650	1320	1588	0.83
SW@650	1334	1598	0.83
NE@650	1320	1598	0.82
SS@650	1336	1599	0.83
NC@750	1347	1594	0.84
NW@750	1348	1595	0.85
SE@750	1348	1594	0.85
SW@750	1347	1594	0.85
NE@750	1348	1595	0.84
SS@750	1347	1594	0.85
NC@850	1320	1598	0.84
NW@850	1320	1598	0.82
SE@850	1400	1598	0.87
SW@850	1400	1598	0.87

NE@850	1300	1597	0.81
SS@850	1400	1600	0.88

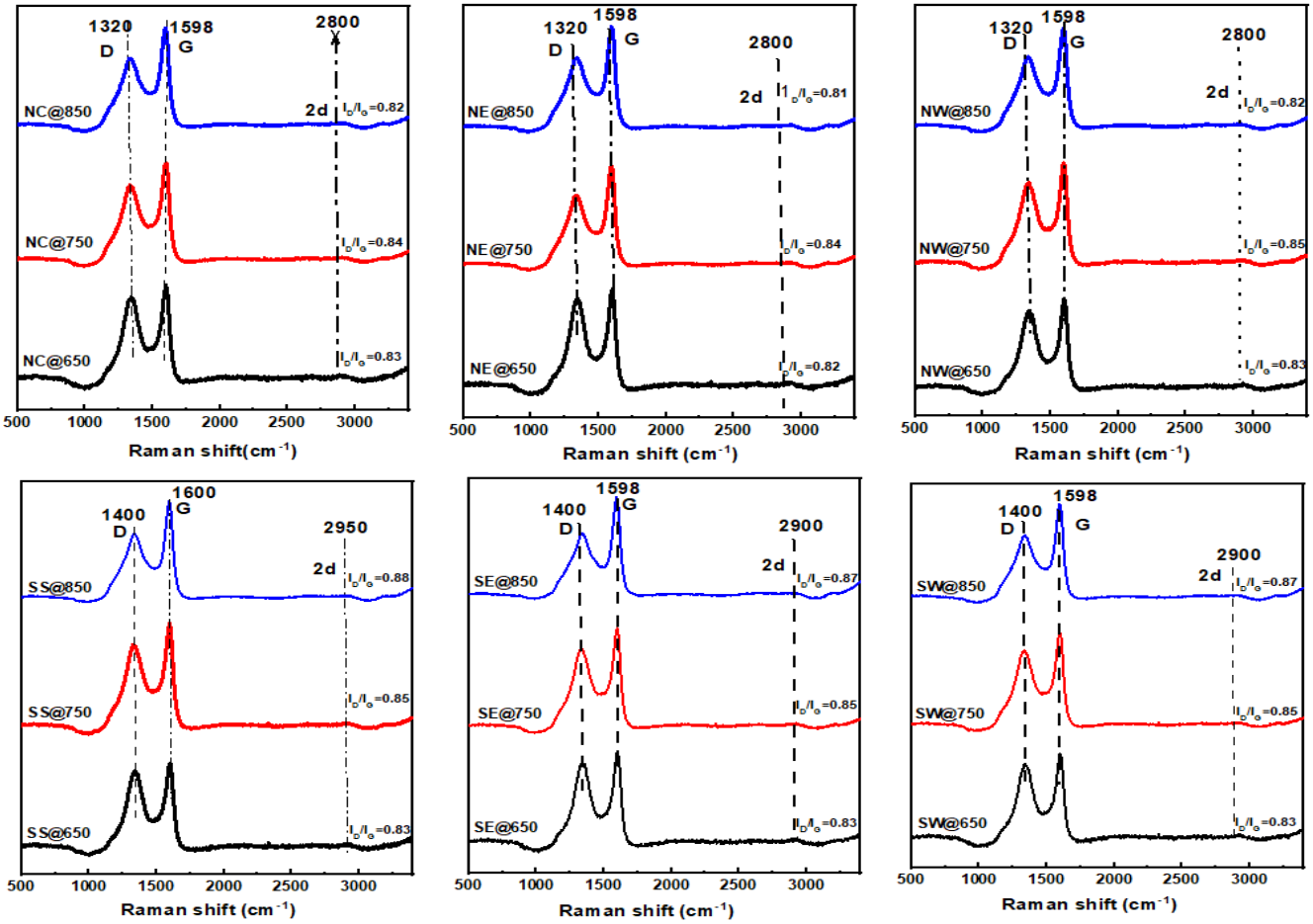

Figure 5: Raman spectra of activated carbon (ACB-H2SO4) with varying pyrolysis temperature 650℃, 750℃ and 850℃

Raman Analysis

The Raman spectra of Cocos nucifera, the plant used to make activated carbon, shows two distinct and well-defined peaks that correspond to the G and D bands, respectively. With pyrolysis temperature at 850°C, the relative intensity ratio of the D band to the G band was found to be 0.87 in the province with higher relative humidity and 0.83 in the province with lower relative humidity. This ratio can indicate a disordered carbon structure or anomalies in the lattice spacing. Higher graphitization and an amorphous character of the carbon material are suggested by a D/G ratio of 0.84. This observation aligns with the results obtained using X-ray diffraction (XRD**).**

Table 3: BET surface area and pore volume of activated carbon prepared in inert! atmosphere.

SAMPLES	$BET\ m^2/g$	$pore\ size\ nm$	$pore\ volume\ cm^3/g$	$R/H(\%)$
NC@650	4.2035	51.07511	0.0366	65
NW@650	2.3441	38.33204	0.0210	35
SE@650	9.5459	22.42046	0.0435	81
SW@650	2.9613	23.1424	0.0280	85
NE@650	3.6736	32.6943	0.0392	38
SS@650	1.0378	89.38787	0.0231	85
NC@750	5.5064	130.66657	0.0221	65
NW@750	2.7513	38.3320	0.0363	35
SE@750	1.8019	85.97908	0.038731	81

SW@750	5.0278	28.9782	0.0364	85
NE@750	3.9051	48.8151	0.0458	38
SS@750	4.649	28.18817	0.0542	85
NC@850	0.7099	26.19945	0.0151	65
NW@850	0.2779	255.9395	0.0177	35
SE@850	13.3512	12.0946	0.0503	81
SW@850	9.6412	23.1424	0.0557	85
NE@850	1.3023	57.67896	0.0131	38
SS@850	7.8812	20.1101	0.0542	85

Strengthening the evidence supporting the carbon structure's amorphous nature by using the complementing data from Raman spectroscopy. The grade of the carbon produced is determined by the moisture content of the coconut shell (Ajien et al., 2023). Lower water (RH) content activated carbon is less graphitized than higher moisture (RH) content activated carbon. Furthermore, using the equation that describes a variety of carbonaceous materials, the degree of graphitization has been determined. The second peak, or G-peak, shows the presence of C=C stretching vibrations, whereas the D-peak is indicative of lattice flaws, edge faults, untidy alignment, and low-symmetry graphitic structure in activated carbon material. The presence of few-layered carbon material and the graphitic nature are shown by (2D), which is caused by the overtone of carbon.

$$R = \frac{I_D}{I_G} \quad (4)$$

where R, I_D, and I_G stand for the graphitization degree, the positioned D-peak intensity, and the positioned G-peak intensity, respectively. Following computation, the value of R was determined to be approximately (0.84-0.087), indicating a somewhat higher graphitization index (Liu et al., 2022).

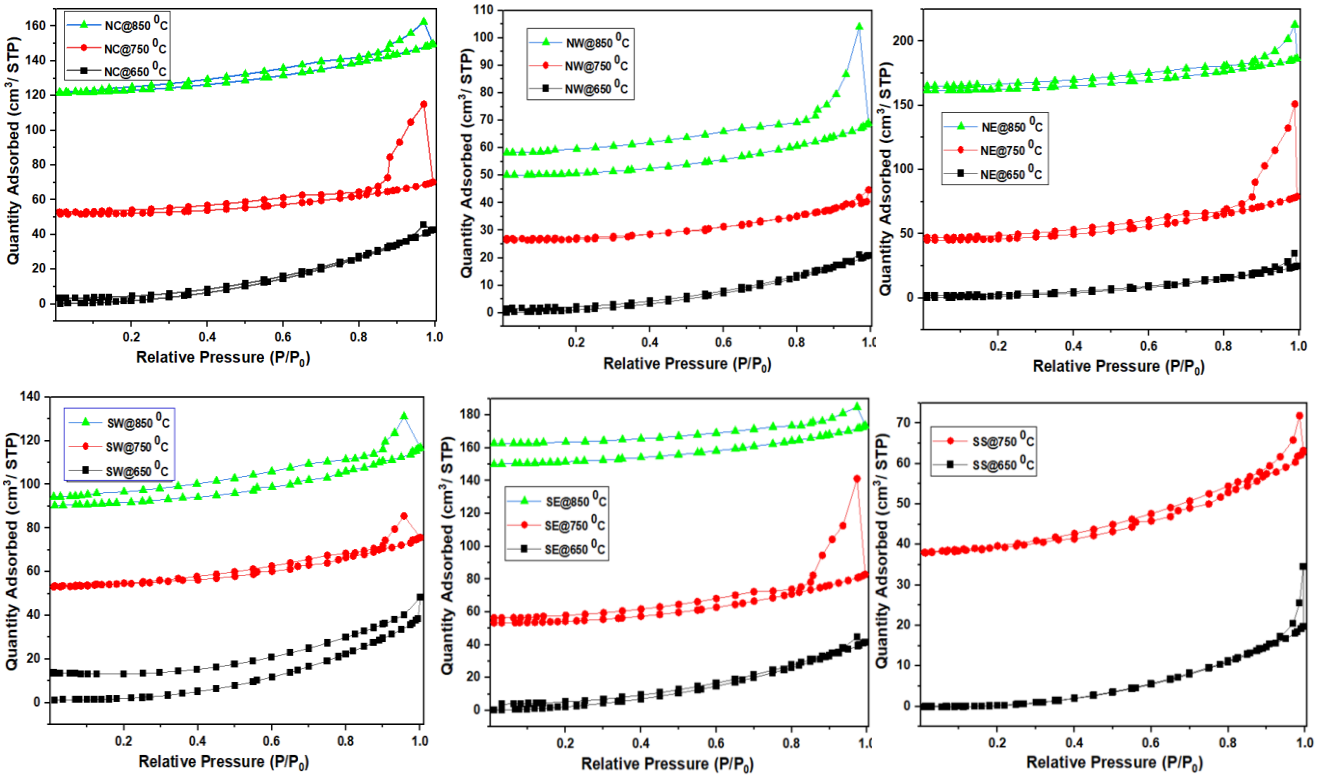

Figure 6: Activation cocos nucifera manufactured in an inert atmosphere with different activation temperature and moisture content: nitrogen adsorption and desorption isotherm

Analysis of the activated carbon's pore size and BET surface

As illustrated in figure 6, the nitrogen adsorption-desorption isotherms of these activated carbons tell an intriguing tale that is concealed inside their complex pore structure. The International Union of Pure and Applied Chemistry (IUPAC) categorization places them in Type (I–IV) category. The secret to comprehending these materials' extraordinary adsorption capability lies in their nature. At these low pressures, remarkable high nitrogen uptakes have been seen as a result of this micropore magic This correlate to these activated carbons' remarkable capacity to absorb different gases, contaminants, and even liquids from their environment. Imagine them as little vacuum cleaners that pick out and retain undesirable molecules. The characterization of activated carbon products requires the use of BET and FESEM investigations, which yield information on the volume and area of micropores, the distribution of pore sizes, and the total surface area. The effects of relative humidity and activation temperature on the different properties of the activated carbon samples are shown in Table 1. This study shows that relative humidity and activation temperature have a synergistic influence on the development of porosity in activated carbon samples. Raising the activation temperature over 650°C greatly increased the specific surface area (micropore, mesopore, and BET surface area) and pore volume (micropore, mesopore, and total pore volume) in both low- and high-humidity settings. The activation process, which encourages the devolatilization of precursor carbon, enlargement of already-existing holes, and formation of new micro- and mesopores, is responsible for this observed tendency. The combined effects of relative density, moisture content, and activation temperature on the textural characteristics of activated carbon were examined in this work. It's interesting to note that depending on the precursor's initial relative density, different temperatures were ideal for optimizing pore volume and BET surface area. Table 1 indicates that samples with a higher density reached their peak values at 850°C, while samples with a lower density reached their maximum at 750°C. The differences in moisture content in the precursors were the reason given for this mismatch. Increases in temperature above 750°C had a detrimental effect on pore volume and surface area in low-moisture samples. In the end, this enhanced porosity results in activated carbon with a higher capacity for adsorption and possible uses in a number of industries.

FESEM analysis

Scanning electron microscopy (FESEM) pictures of activated carbon generated in an inert environment at different humidity and temperature levels are shown in Figure 5. The variations in surface morphology at 650, 750, and 850 °C activation temperatures are depicted in these photos. We can see how the humidity and activation temperature affect the physical properties of carbon by magnifying it 10,000 times. This thorough investigation offers insightful information about the complex microstructure of the activated carbons, which is marked by a wide variety of pore sizes and shapes and the material's potential for a number of uses, including energy storage, adsorption, and catalysis. Carbonization caused a chemical exodus that resulted in the formation of complex webs of pores on the outside of the activated carbons. These compounds gave up their previous spaces as they evaporated, resulting in the emergence of many pores of various sizes.

The surface morphology of activated carbon synthesized in an inert atmosphere with low humidity is shown in Figure 5(a-c). A porous structure with a variety of pore sizes and shapes is shown via microscopy. Nonetheless, pore size decreases and the microstructure become more disintegrated as the carbonization temperature is raised to 850°C. As opposed to drier samples, activated carbon made with higher humidity displays larger pores as well as an intriguing feature: these larger pores are arranged in a well-defined, structured manner rather than randomly.

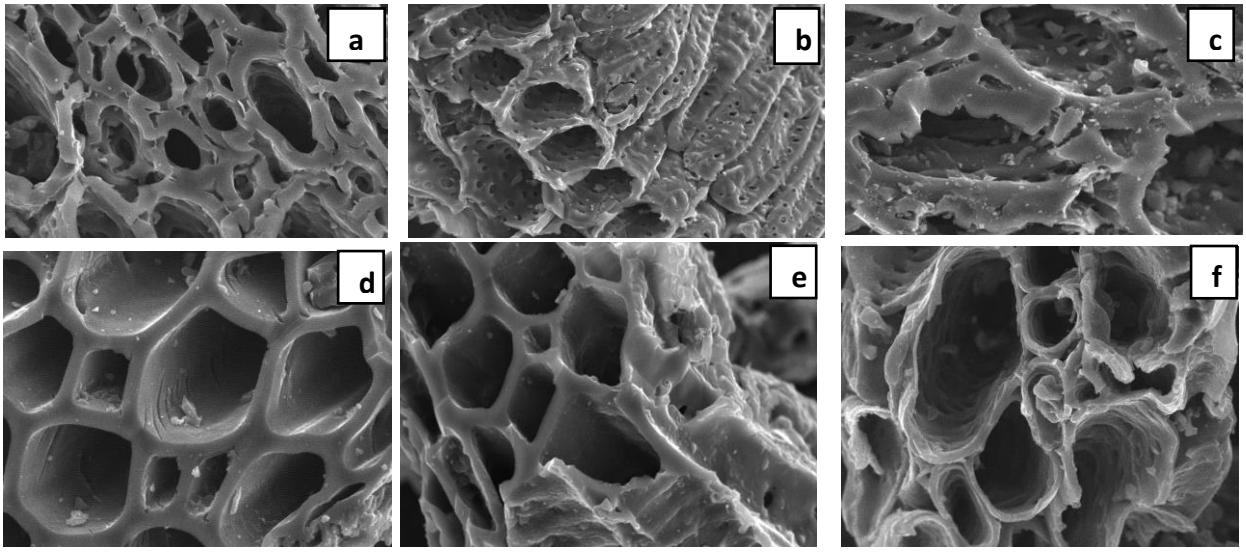

Figure 7: Images captured by a FESEM show the complex surface structures of activated carbon formed at varied (10000X) temperatures (650°C, 750°C, and 850°C) and humidity levels (low and high). The photographs in sets (a, b, and c) depict the North-West orientation, whereas the sets (d, e, and f) provide the South-East and South-West views

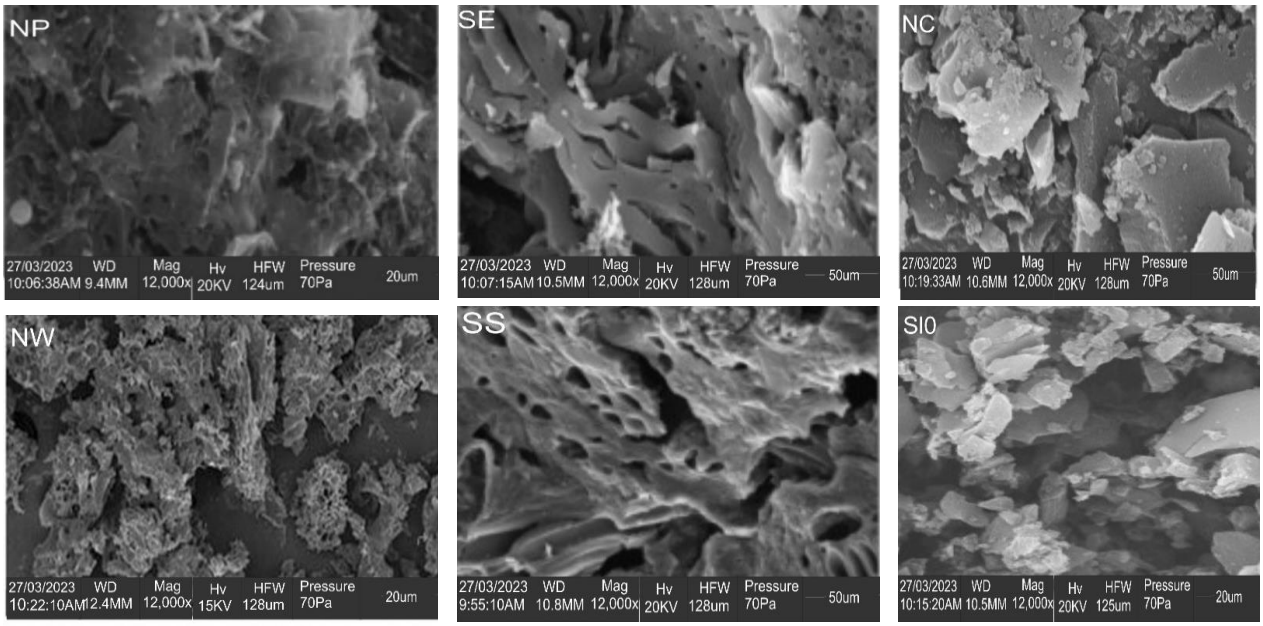

Figure 8: SEM-EDS in situ pictures with varying humidity levels (high and low). The North-West orientation is represented by each set of photographs (a, b, c), while the South-East and South-West viewpoints are shown in (d, e, f)

CONCLUSION

In Conclusion, this study has demonstrated the critical role of relative humidity in influencing the properties of activated carbon, alongside established parameters such as temperature and impregnation. The findings suggest that higher humidity can lead to increased moisture content, but surprisingly, it can also boost surface area for samples carbonized at higher temperatures. This study has significant implications for optimizing activated carbon production from readily available coconut shells, as it paves the way for economical and diverse applications. By considering humidity alongside traditional parameters, this study has successfully accomplished its overarching goal and objectives, creating activated carbon samples from diverse regions in Nigeria, analyzing their structural and molecular properties, and evaluating their morphological and porosity features at different pulverization temperatures.

REFERENCES

Abdullah, S., Zubir, M. N. B. M., Muhamad, M. R. B., Newaz, K. M. S., Öztop, H. F., Alam, M. S., & Shaikh, K. (2023). Technological development of evaporative cooling systems and its integration with air dehumidification processes: A review. *Energy and Buildings*, 112805. doi.org/10.1016/j.enbuild.2023.112805

Ajien, A., Idris, J., Md Sofwan, N., Husen, R., & Seli, H. (2023). Coconut shell and husk biochar: A review of production and activation technology, economic, financial aspect and application. *Waste Management & Research*, *41*(1), 37-51.

Chowdhury, Z. Z., Karim, M. Z., Ashraf, M. A., & Khalid, K. (2016). Influence of carbonization temperature on physicochemical properties of biochar derived from slow pyrolysis of durian wood (Durio zibethinus) sawdust. *BioResources*, *11*(2), 3356-3372.

Chen, X., Zhang, J., Zhang, B., Dong, S., Guo, X., Mu, X., & Fei, B. (2017). A novel hierarchical porous nitrogen-doped carbon derived from bamboo shoot for high performance supercapacitor. *Scientific reports*, *7*(1), 7362.
doi: 10.1038/s41598-017-06730-x

Cotrina Cabello, G. G., Ruiz Rodriguez, A., Husnain Gondal, A., Areche, F. O., Flores, D. D. C., Astete, J. A. Q., . & Cruz Nieto, D. D. (2023). Plant adaptability to climate change and drought stress for crop growth and production. *CABI Reviews*, (2023).
doi: 10.1079/cabireviews.2023.0004

Das, D., Samal, D. P., & Meikap, B. C. (2015). Preparation of activated carbon from green coconut shell and its characterization. *J. Chem. Eng. Process Technol*, *6*(5), 1000248.
doi: 10.4172/2157-7048.1000248

De Groeve, M., Kale, E., Orr, S. A., & De Kock, T. (2023). Preliminary Experimental Laboratory Methods to Analyse the Insulation Capacity of Vertical Greening on Temperature and Relative Humidity. *Sustainability*, *15*(15), 11758. doi: 10.3390/su151511758

Dhillon, R. S., & von Wuehlisch, G. (2013). Mitigation of global warming through renewable biomass. *Biomass and bioenergy*, *48*,75-89.

Onwumelu, D. C. (2023). Biomass-to-power: Opportunities and challenges for Nigeria. *World Journal of Advanced Research and Reviews*, *20*(2), 001-023.
doi: 10.1016/j.biombioe.2012.11.005

Elmouwahidi, A., Bailón-García, E., Pérez-Cadenas, A. F., Maldonado-Hódar, F. J., & Carrasco-Marín, F. (2017). Activated carbons from KOH and H3PO4-activation of olive residues and its application as supercapacitor electrodes. *Electrochimica Acta*, *229*, 219-228. doi: 10.1016/j.electacta.2017.01.152

Fang, Z., Huiying jiang, Qiu, W., Jiang, Z., Peng, Z., Tian, K., ... & Li, X. (2023). Lithium/Sodium Deposition Behavior and Dendrite Inhibition Mechanism on Metal-Modified and Nitrogen-Doped Carbon Nanotube Skeletons. *The Journal of Physical Chemistry C*, *127*(6), 2835-2845. doi: 10.1021/acs.jpcc.2c07797

Foo, K. Y., & Hameed, B. H. (2012). Coconut husk derived activated carbon via microwave induced activation: effects of activation agents, preparation parameters and adsorption performance. *Chemical Engineering Journal*, *184*, 57-65.
doi: 10.1016/j.cej.2011.12.084

Gao, F., Qin, S. H., Zang, Y. H., Gu, J. F., & Qu, J. Y. (2020). Highly efficient formation of Mn3O4-graphene oxide hybrid aerogels for use as the cathode material of high performance lithium ion batteries. *New Carbon Materials*, *35*(2), 121-130.doi: 10.1016/S1872-5805(20)60479-6

Hall, P. J., Mirzaeian, M., Fletcher, S. I., Sillars, F. B., Rennie, A. J., Shitta-Bey, G. O., ... & Carter, R. (2010). Energy storage in electrochemical capacitors: designing functional materials to improve performance. Energy & Environmental Science, 3(9), 1238-1251.
doi: 10.1039/C0EE00004C

Jiang, Z. H., Yang, Z., So, C. L., & Hse, C. Y. (2007). Rapid prediction of wood crystallinity in Pinus elliotii plantation wood by near-infrared spectroscopy. Journal of wood science, 53, 449-453.

Kumagai, S., Sato, M., & Tashima, D. (2013). Electrical double-layer capacitance of micro-and mesoporous activated carbon prepared from rice husk and beet sugar. *Electrochimica acta*, *114*, 617-626.
doi: 10.1016/j.electacta.2013.10.060

Lekakou, C., Moudam, O., Markoulidis, F., Andrews, T., Watts, J. F., & Reed, G. T. (2011). Carbon-based fibrous EDLC capacitors and supercapacitors. *Journal of Nanotechnology*, *2011*. doi: 10.1155/2011/409382

Lee, Y. J., Kim, G. P., Bang, Y., Yi, J., Seo, J. G., & Song, I. K. (2014). Activated carbon aerogel containing graphene as electrode material for supercapacitor. *Materials Research Bulletin*, *50*, 240-245.doi:

10.1016/j.materresbull.2013.11.021 doi: 10.4172/2157-7048.1000248

Liu, R., Yang, J., Liu, R., Tang, Y., Huang, L., & Shuai, Q. (2022). Effects of Nanopore Size on the Adsorption of Sulfamerazine from Aqueous Solution by β-Ketoenamine Covalent Organic Frameworks. *ACS Applied Nano Materials*, *5*(12), 17851-17858. doi: org/10.1021/acsanm.2c03806

Mahmoud, S. H., Gan, T. Y., & Zhu, D. Z. (2023). Impacts of climate change and climate variability on water resources and drought in an arid region and possible resiliency and adaptation measures against climate warming. *Climate Dynamics*, 1-27. doi: 10.1007/s00382-023-06795-7

Masthura, E., & Abdul, H. D. (2018). Effects of activation temperature on characteristics and microstructure of coconut shell-based activated carbon. *Eurasian J. Anal. Chem*, *4*(13), 384-390 doi:10.1039/C000417K

Nankya, R., Opar, D. O., Kim, M. J., Paek, S. M., & Jung, H. (2020). Synergetic effect of nitrogen and sulfur co-doping in mesoporous graphene for enhanced energy storage properties in supercapacitors and lithium-ion batteries. *Journal of Solid State Chemistry*, *289*, 121451. doi:10.1016/j.jssc.2020.121451

Ozoemena, K. I., & Chen, S. (Eds.). (2016). *Nanomaterials in advanced batteries and supercapacitors* (p. 423). Switzerland: Springer. doi: 10.1007/978-3-319-26082-2

Rippel, T. M., Mooring, E. Q., Tomasula, J., & Wimp, G. M. (2020). Habitat edge effects decrease litter accumulation and increase litter decomposition in coastal salt marshes. *Landscape Ecology*, *35*, 2179-2190. doi: 10.1007/s10980-020-01108-3

Roberts, K. G., Gloy, B. A., Joseph, S., Scott, N. R., & Lehmann, J. (2010). Life cycle assessment of biochar systems: estimating the energetic, economic, and climate change potential. *Environmental science & technology*, *44*(2), 827-833. doi: 10.1021/es902266r

Sahu, A., Sen, S., & Mishra, S. C. (2023). A comparative study on characterizations of biomass derived activated carbons prepared by both normal and inert atmospheric heating conditions. *Journal of the Indian Chemical Society*, *100*(4), 100943. doi: 10.1016/j.jics.2023.100943

Sammed, K. A., Farid, A., Mustafa, S., Kumar, A., Tabish, M., Khan, A. A., & Zhao, W. (2023). Developing next-generation supercapacitor electrodes by coordination chemistry-based advanced functional carbon nanostructures: Progress, Current challenges and prospects. *Fuel Processing Technology*, *250*, 107896. doi: 10.1016/j.fuproc.2023.107896

ván, B., Juan, P., Luciana, A., Morales, J. M., & Thomas, K. (2023). Microclimate and species composition shape the contribution of fuel moisture to positive fire-vegetation feedback. *Agricultural and Forest Meteorology*, *330*, 109289. doi: 10.1016/j.agrformet.2022.109289 doi: 10.1002/adma.201100984

Yakout, S. M., & El-Deen, G. S. (2016). Characterization of activated carbon prepared by phosphoric acid activation of olive stones. *Arabian journal of chemistry*, *9*, S1155-S1162. doi: 10.1016/j.arabjc.2011.12.002

Yang, X., He, H., Lv, T., & Qiu, J. (2023). Fabrication of biomass-based functional carbon materials for energy conversion and storage. *Materials Science and Engineering: R: Reports*, *154*, 100736. doi: 10.1016/j.mser.2023.100736

Zhai, Y., Dou, Y., Zhao, D., Fulvio, P. F., Mayes, R. T., & Dai, S. (2011). Carbon materials for chemical capacitive energy storage. *Advanced materials*, *23*(42), 4828-4850.

Zhang, J., Jin, X., & Yang, C. (2022). Efficient removal of organic pollutants in waste sulfuric acid by an advanced oxidation process using coconut shell-derived biochar to produce qualified poly aluminium sulfate. *Separation and Purification Technology*, *293*, 121057. doi: 10.1016/j.seppur.2022.121057

Zhang, L. L., Zhou, R., & Zhao, X. S. (2010). Graphene-based materials as supercapacitor electrodes. *Journal of Materials Chemistry*, *20*(29), 5983-5992.

Zhang, Y., Zhang, Y., Lian, X., Zheng, Z., Zhao, G., Zhang, T., ... & Piao, S. (2023). Enhanced dominance of soil moisture stress on vegetation growth in Eurasian drylands. *National Science Review*, nwad108. doi: 10.1093/nsr/nwad108